PZT-BASED ENERGY HARVESTERS ON PLASTIC FOIL OPTIMIZED THROUGH THEORETICAL MODELING AND FABRICATION IMPROVEMENTS

Nadine Besse*, Andrés Vásquez Quintero, Danick Briand†, Pattanaphong Janphuang, Robert Lockhart, Jinyu J. Ruan, and Nico F. de Rooij

Ecole Polytechnique Fédérale de Lausanne (EPFL), Institute of Microengineering (IMT)
Sensors, Actuators and Microsystems Laboratory (SAMLAB), Neuchâtel, Switzerland
*Presenting Author, †Contacting Author: danick.briand@epfl.ch

Abstract: Thinned bulk-PZT cantilever-based vibration energy harvesters with a tungsten tip-mass, transferred by low-temperature lamination processes onto a plastic substrate, are presented in this paper. In order to optimize their performances, correlations between theoretical models and experimental measurements have been implemented. Both analytical and FEM simulations in COMSOL have been combined to obtain a global and complete model emulating the real system behavior. As a result, an optimized device, resonating at at 41.1 Hz and able to generate an average power of 63.7 μW and a normalized power density of 3472 $\mu W/g^2 \cdot cm^3$ at 1 g, was obtained.

Keywords: piezoelectric energy harvesters, thinned bulk-PZT, plastic substrate

INTRODUCTION

The recent development of ultra-low-power flexible smart wireless devices has encouraged researchers to investigate energy harvesters on plastic foils (solar, mechanical, thermal). Few approaches have been introduced to produce piezoelectric flexible mechanical energy harvesters have been reported in the literature: inserting a multilaminar polyvinylidene-fluoride (PVDF) layer into a shoe [1]; transferring lead-zirconate-titanate (PZT) nanoribbons onto flexible polydimethylsiloxane (PDMS) rubber [2]; aligning zinc-oxide (ZnO) nanowires arrays on polyimide (PI) [3] or depositing ZnO onto polyethylene-terephthalate (PET) [4]. In [5], our group proposed to transfer thinned bulk-PZT by lamination onto a PET substrate. By combining the performing bulk-PZT material [6] with a plastic cantilever, the resonant frequency of the harvesters can be lowered and cost-effective devices can be manufactured compared to silicon-based harvesters, while still maintaining interesting power densities.

In this work, the optimization of the energy harvesters reported in [5] was investigated by combining modeling and experiments. A theoretical model, comprising correlations between analytical, FEM simulations in COMSOL and experiments, was developed. Consistency is ensured by implementing a Euler-Bernoulli analysis of the beam motion, calculating the back-coupling effect, emulating the measured damping trend and computing the additional stress-charges generated in the extra-electrode area at the anchor point.

The outcome of this work is optimized energy harvesters composed by a thinned bulk-PZT layer onto a PET cantilever with a tungsten tip-mass exhibiting resonance in the low frequency range (10 Hz to 100 Hz), with an improvement by a factor of 5 to 10 in absolute power generated and normalized power density compared to [5].

DESIGN AND FABRICATION

The vibration energy harvesters use a unimorph cantilever configuration with a rectangular cross-sectional area composed by three distinguishable layers and a tip-mass. A polymeric foil in PET, 125 μm thick (Melinex® ST506 from DuPont™), is used as the substrate. The active piezoelectric material is a PZT sheet thinned down from 125 μm (PZT-5H from Piezo System Inc.) to 75 μm to improve the performance of the harvesters. Both PET and PZT layers are bonded together with a 14 μm thick epoxy-based dry film photoresist (PerMX™ 3050 from DuPont™). The devices are fixed on a rigid printed circuit board (PCB) frame for handling and measurement purposes. Finally, a tungsten mass of 500 μm thick is fixed on the tip with a dry adhesive (ARClear® 8932 from Adhesives Research Inc.) to reduce the resonant frequency and enhance the output power of the system.

The fabrication process has already been reported in detail by our group in [5] and thus only the four main steps will be pointed out in this paper. The entire process is performed at low temperature ($<85^{\circ}$C) to be compatible with the polymeric substrate used.

To begin, all of the materials are patterned to their respective final shapes. Before being patterned using a standard dicing process, the bulk-PZT, fixed on a sili-

con wafer, is thinned down by grinding until its desired thickness. Then a chromium/nickel layer is re-deposited to replace the top metallic contact lost in the thinning process. The PET substrate, the tungsten tip-mass and the PCB rigid support are all patterned using a computer numerical control (CNC) drill. In the future, laser ablation could be used instead to avoid burrs and improve the compatibility with large scale production.

Next, a dry film photoresist is used to transfer the piezoelectric layer onto the plastic substrate. It is first laminated on the PZT cantilever at low temperature (85°C). Then, both are aligned and bonded to the PET substrate by applying pressure and heat (2 bars at 85°C).

Once assembled, the three-layered cantilever is fixed on the rigid support with a dry adhesive film and electrically connected to the PCB frame. The bottom electrode is connected with a silver-based conductive glue through the hole designed in the substrate. The top electrode is directly connected by soldering.

Finally, the tungsten mass is aligned carefully on the tip of the cantilever and fixed using a dry adhesive. A fully fabricated device is illustrated in Figure 1.

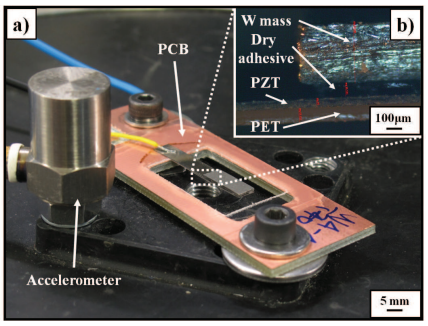

Fig. 1: Photographs of the energy harvester. (a) Global view of the device, (b) Cross-section of the beam.

THEORETICAL MODELING

The behavior of the vibration energy harvesters was studied using an analytical model which was developed based on several models reported in the literature [7–9]. The theoretical model is obtained by combining: 1) the Euler-Bernoulli analysis of the beam motion; 2) the consideration of the mass as an inertial body; 3) the implementation of the back-coupling effect; 4) the measurement of damping trend and 5) the understanding through simulations in COMSOL of the additional stress-charges generated in the extra electrode area. Only steps 3), 4) and 5) will be detailed below, since they bring new and interesting information about the operation of the system. A schematic illustrating the modeling is given in Figure 2.

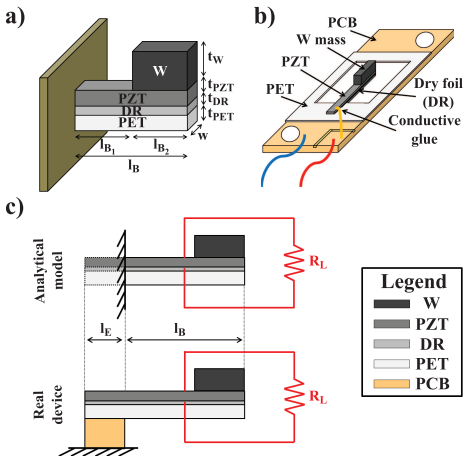

Fig. 2: Schematics of the device. (a) Main dimensions of the system, (b) Global schematic of the device, (c) Comparison between the real device structure and its analytical modeling.

The final formula obtained for the output power is given by the nested equations in Equation 1, in which $\omega_{b,n}$ are the base and natural pulsation, respectively, R_L is the load resistance, C is the capacitor, Q is the amount of stress-charge generated, m is the cross-sectional mass, a is the acceleration, $l_{E,B}$ are the extra-electrode and beam lengths, w is the width, t_{PZT} is the PZT thickness, h is the neutral plane location from the bottom of the piezoelectric layer, ζ is the damping coefficient, K is the back-coupling parameters, α is the correction factor for the additional stress-charges generated, X_n is the spatial deflection of the beam and φ and γ are two parameters used to simplify the notation.

$$
\begin{aligned}
P &= \frac{R_L\cdot\omega_b^2\cdot(Q_1+Q_2)^2\cdot\gamma^2/2}{\left[\omega_n^2-\omega_b^2-2\cdot\zeta\cdot\omega_n\cdot\omega_b^2\cdot R_L\cdot C\right]^2+\left[\omega_b\cdot R_L\cdot(Q_1+Q_2)\cdot\varphi+\left(\omega_n^2-\omega_b^2\right)\cdot\omega_b\cdot R_L\cdot C+2\cdot\zeta\cdot\omega_n\cdot\omega_b\right]^2} \\
C &= \varepsilon_0\cdot\varepsilon\cdot\frac{w\cdot(l_E+l_B)}{t_{PZT}} \qquad K_{1,2} = -E_{PZT}\cdot d_{31}\cdot(t_{PZT}/2-h_{1,2}) \\
\gamma &= \frac{\sum m_{1,2}\cdot a\cdot\int_0^{l_{B1,2}} X_n(x)\cdot dx}{\sum m_{1,2}\cdot\int_0^{l_{B1,2}} X_n^2(x)\cdot dx} \qquad \varphi = \frac{\sum K_{1,2}\cdot\int_0^{l_{B1,2}}\frac{d^2X_n(x)}{dx^2}\cdot dx}{\sum m_{1,2}\cdot\int_0^{l_{B1,2}} X_n^2(x)\cdot dx} \\
Q_{1,2} &= -\frac{\alpha}{t_{PZT}}\cdot\int_0^{l_{B1,2}}\int_0^{w}\int_{-h_{1,2}}^{t_{PZT}-h_{1,2}} d_{31}\cdot E_{PZT}\cdot z\cdot\frac{d^2X_n(x)}{dx^2}\cdot dx\cdot dy\cdot dz
\end{aligned}
\tag{1}
$$

Back-coupling effect

The back-coupling effect is an intrinsic property of piezoelectric materials. In fact, the generation of stress-charges creates local voltage potentials and thus small Lorentz forces inside the structure which counteract the beam displacement. This phenomenon, represented by the coefficient K in Equation 1, depends on the position of the neutral plane with respect to the middle of the PZT layer. Therefore, as shown in Figure 3, it will always be more influential in silicon-based systems compared to plastic-based systems of equal dimensions.

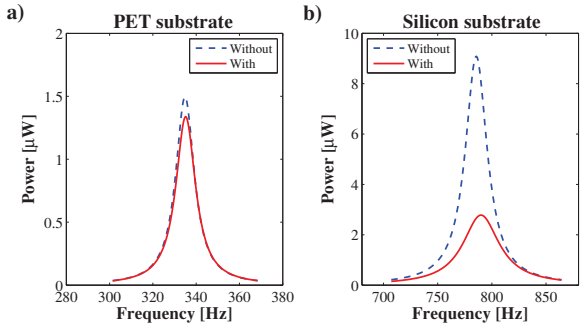

Fig. 3: Theoretical influence of back-coupling on two devices of equal dimensions. (a) Plastic-based device, (b) Silicon-based device.

Damping trend

In order to understand the effects of damping, and thereby accurately simulate the system behavior at different accelerations, damping values were measured on devices fabricated with various dimensions. It has been observed that losses are mainly due to internal structural friction, implying a direct influence of acceleration, but less form the area. The results obtained are represented in Figure 4.

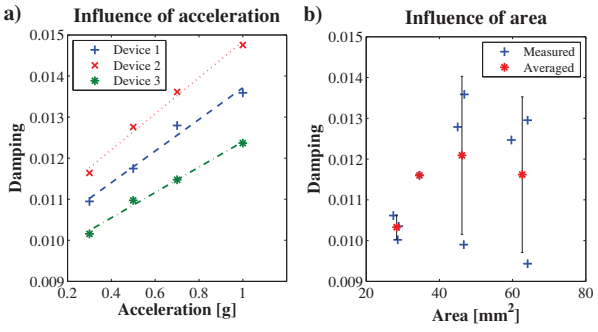

Fig. 4: Measured damping tendency on a set of devices. (a) Influence of the acceleration on three devices, (b) Influence of the area measured at 1 g.

Additional stress-charges

In a piezoelectric cantilever-based system, some of the PZT extends beyond the mechanical clamping region in order to create a high stress gradient and generate charges. The extra PZT area, not included in the perfectly clamped system, increases the capacitance and adds additional stress-charges which modifies the system behavior. Therefore, the analytical model requires a correction factor to take the additional stress-charges into account. Values of $\alpha = 1.10 - 1.15$ were found for the studied PZT plastic-based systems using COMSOL simulations as a reference.

Model validation

In order to demonstrate the validity of the analytical model, experimental and theoretical powers are compared in Figure 5. At high acceleration, the beam enters in a non-linear regime since large deformations are implied (noticeable by a change in the shape of the transfer function), which limits the model accuracy. Another approach, using non-linear elastic, coupling and damping coefficients, was recently proposed by [10] to take these non-conservative phenomena into account.

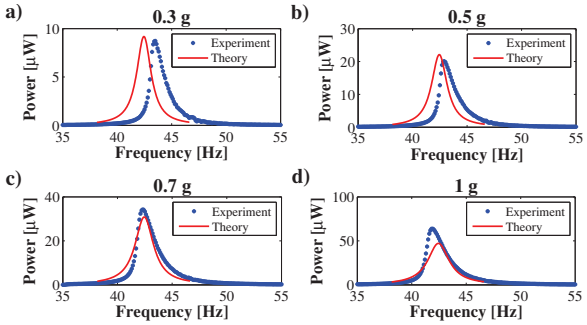

Fig. 5: Comparison between theoretical and experimental performances of the optimized device at different accelerations: (a) 0.3 g, (b) 0.5 g, (c) 0.7 g and (d) 1 g.

OPTIMIZATION

The model described previously was used to optimize five parameters: the beam length and width, the PZT thickness, the PZT/PET and the Mass/Beam length ratios. As shown in Figure 6, the conclusion is that a long and wide PET cantilever entirely covered by a thinned bulk-PZT sheet with a tungsten mass on the second half of the beam presents the best performances.

Optimal device

Experimentally, the best device is 19.7 mm long, 1.9 mm wide and 125 μm – 14 μm – 70 μm thick (PET – DR – PZT), with a tungsten mass 10 mm long, 2.2 mm wide and 500 μm thick placed on the tip. Longer, wider and thinner devices have been fabricated which presented better experimental performances without mass, but they broke during testing with a tip-mass due to the high fragility of the beams and especially of

the thinned bulk-PZT layers.

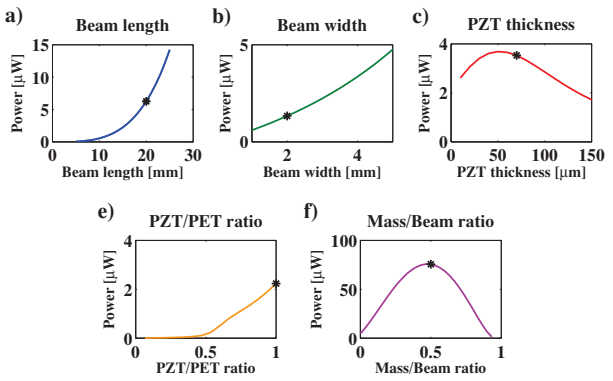

Fig. 6: Optimization of five different parameters: (a) Beam length, (b) Beam width, (c) PZT thickness, (d) PZT/PET length ratio and (e) Mass/Beam length ratio. Dimensions of the best device represented by (*).

At 1 g, the system experimentally delivers an average power of 63.7 μW and resonates at 41.1 Hz with a 3dB-bandwidth of 2.2 Hz, resulting in a normalized power density (N.P.D.) of 3472 $\mu W/g^2 \cdot cm^3$, a volume figure of merit (FoM_V) of 4.31 % and a bandwidth figure of merit (FoM_{BW}) of 0.11 % as defined by [11]. It implies an improvement by a factor of 5 to 10 in absolute power and normalized power density compared to the previous publication [5]. The transfer function is illustrated in Figure 7.

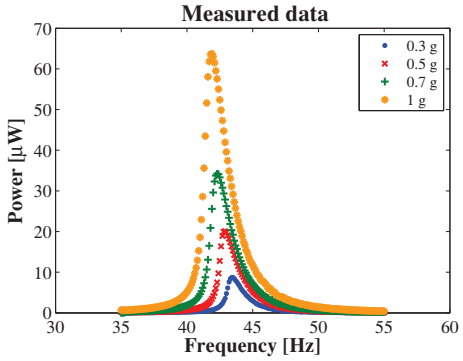

Fig. 7: Measured performances of the best device at different accelerations (0.3 g to 1 g).

CONCLUSION

A theoretical model, comprising correlations between analytical, FEM simulations and experiments, has been developed to optimize the system simply and smartly. Consequently, a device able to generate 63.7 μW at 1 g, resulting in a N.P.D. of 3472 $\mu W/g^2 \cdot cm^3$, was obtained.

In the future, further improvements in terms of power could be achieved by investigating piezoelectric energy harvesters with a bimorph configuration. Similar fabrication processes, especially lamination of bulk materials, should be used to ensure high performances. However, the stability over time of plastic beams needs to be studied and the fabrication process should be improved by replacing the CNC drilling by a laser ablation step.

REFERENCES

[1] Shenck N. and Paradiso J. 2001 Energy Scavenging with Shoe-Mounted Piezoelectric *IEEE Micro* **21** 30–42

[2] Qi Y., Jafferis N. T., Lyons K., Lee C. M., Ahmad H. and McAlpine M. C. 2010 Piezoelectric Ribbons Printed onto Rubber for Flexible Energy Conversion *Nano Letters* **10** 524–528

[3] Zhu G., Yang R., Wang S. and Wang Z. 2010 Flexible High-Output Nanogenerator Based on Lateral ZnO Nanowire Array *Nano Letters* **10** 3151–3155

[4] Pan C. T., Liu Z. H., Chen Y. C., Chang W. T. and Chen Y. J. 2011 Study of Vibration-Induced Broadband Flexible Piezoelectric ZnO Micro-Harvester with Storage System *Transducers'11* (*Beijing, China, June 2011*) 1669–1672

[5] Vásquez Quintero A., Briand D., Janphuang P., Ruan J. J., Lockhart R. and de Rooij N. F. 2012 Vibration Energy Harvester on Plastic Foil by Lamination of PZT Thick Sheets *MEMS 2012* (*Paris, France, February 2012*) 1289–1292

[6] Aktakka E. E., Peterson R. L. and Najafi K. 2011 Thinned-PZT on SOI Process and Design Optimization for Piezoelectric Inertial Energy Harvesting *Transducers'11* (*Beijing, China, June 2011*) 1649–1652

[7] Priya S. and Inman D. J. 2008 *Energy Harvesting Technologies, Ch.* 2 (New-York, USA: Springer)

[8] Piersol A. G. and Paez T. L. 2009 *Harris' Shock and Vibration Handbook (6th Ed.), Ch.* 7 (New-York, USA: McGraw Hill)

[9] Erturk A. and Inman D. J. 2011 *Piezoelectric Energy Harvesting* (Chichester, UK: Wiley)

[10] Stanton S. C., Erturk A., Mann B. P., Dowell E. H. and Inman D. J. 2011 Nonlinear Nonconservative Behavior and Modeling of Piezoelectric Energy Harvesters Including Proof Mass Effects *Journal of Intelligent Material Systems and Structures* **23** 183–199

[11] Mitcheson P. D., Yeatman E. M., Rao G. K., Holmes A. S. and Green T. C. 2008 Energy Harvesting From Human and Machine Motion for Wireless Electronic Devices *Proceedings of the IEEE* **96** 1457–1486